



# Investigation of ZnO nano-filler-dispersed nano-composite polymer electrolytes and their ion transport property

Niranjan Kumar<sup>1</sup> · Manju Sahu<sup>1</sup> · Dinesh K. Sahu<sup>2</sup> · Y. K. Mahipal<sup>1</sup>

Received: 18 April 2022 / Revised: 12 May 2022 / Accepted: 19 May 2022 / Published online: 31 May 2022  
© The Author(s), under exclusive licence to Springer-Verlag GmbH Germany, part of Springer Nature 2022

## Abstract

The present manuscript represents the comprehensive studies of the poly (ethylene oxide)-based sodium ion-conducting solid polymer electrolyte (SPE) and nano-composite polymer electrolyte (NCPE) membranes dispersed with different wt. (%) of ZnO nano-filler that have been synthesized by the hot-press method. This novel method gave rise to flexible, uniform/thin polymer electrolyte films which can be achieved in any desired shape/size. X-ray diffraction (XRD) was used to analyze the structural properties of the SPE host and the NCPE optimum conducting composition (OCC) film. Scanning electron microscopy (SEM) confirmed the smoother surface and energy-dispersive spectroscopy (EDAX) confirmed the presence of all key elements. Thermo-gravimetric analysis (TGA) and differential scanning calorimetry (DSC), respectively, indicated good thermal stability and an improved amorphous phase. The dispersion of the ZnO nano-filler particles has enhanced the ionic conductivity, thermal stability, and also mechanical integrity. Ion transport properties have been characterized by assembling symmetric cells: SS||SPE/NCPE||SS (SS stainless steel), the NCPE OCC membrane exhibits the maximum ionic conductivity ( $\sigma_n$ )  $\sim 1.45 \times 10^{-5}$  S/cm at room temperature, low activation energy ( $E_a \sim 0.35$  eV), and ionic transference number ( $t_{ion} \sim 0.99$ ) close to unity and also the cyclic voltammetry (CV) curve shows the good electrochemical stability so electrolyte has been found more suitable for device fabrication.

**Keywords** Solid polymer electrolyte · Nano-composite polymer electrolyte · Ionic conductivity · A.C. impedance spectroscopy · Thermal properties · Cyclic voltammetry

## Introduction

In the era of advanced technology, the development of renewable energy sources, such as wind, solar, and nuclear energy sources, has become necessary due to the limited availability of traditional fossil fuels [1]. However, with the advancement of renewable energy sources, we have to focus on portable electrical energy storage devices to smooth the intermittency of the energy sources. Battery devices have the potential to provide a solution, especially as they can store energy from renewable energy sources such as wind and solar power. The rechargeable battery can store chemical

energy as well as it can convert it into electrical energy with high efficiency [2, 3]. In the latest technology of electrical energy storage devices, lithium-ion battery (LIB) has been dominating the market of portable electronic devices, electric vehicles, and hybrid electric vehicles due to their high output voltages, high energy densities, and long durability. But due to very high cost, less abundance and the toxic nature of lithium are inhibiting the application of LIB in large-scale energy storage [4–9]. Therefore, many researchers are trying to develop sodium-ion secondary batteries parallelly which could be able to replace Li-ion associated energy storage devices successfully. The most believable and competitive element with comparable performance and very close chemical insertion properties that have the potential to replace lithium (Li) and eliminate the hurdles is sodium (Na). The abundance of sodium resources (1000 times more than Li), low price of starting materials, voltage versus SHE (2.7 V), and low toxicity are favorable for sodium-ion battery (SIB) technology enhancement in industrial applications, viz., portable electronic devices and for electric road

✉ Y. K. Mahipal  
ykmahipal@gmail.com

<sup>1</sup> Solid State Ionics Research Laboratory, School of Studies in Physics & Astrophysics, Pt. Ravishankar Shukla University, Raipur 492010, Chhattisgarh, India

<sup>2</sup> State Forensic Science Laboratory (SFSL), Raipur, Chhattisgarh, India

vehicles [10–14]. The energy density of the SIBs is comparatively low; however, the energy density would not be considered the crucial issue for large-scale grid support, where the low cost of synthesis and the battery durability including long cycle life are the most important parameters [15, 16]. Based on all merits over LIBs, all-solid-state SIBs are regarded as the next-generation battery. Sodium-ion-based solid-state electrolytes should employ rather than the liquid organic electrolytes, which exhibit better thermal/mechanical integrity, superior durability, and enhanced electrochemical stability with desirable shape/size [13, 17–19].

Based on the previous studies, it has been identified that solid polymer electrolyte (SPE) film is suitable for the development of all solid-state SIB [20]. Solid polymer electrolytes have gained tremendous attention in the past four decades due to their potential applications in electrochemical/electrical power generation, energy storage, and conversion systems such as electrochromic displays, sensors, supercapacitors, and rechargeable batteries [21–23]. Later, many polymers have been used for the synthesis of polymer electrolytes. Mainly in the synthesis of the SPEs, high molecular weight polar polymer, viz., poly (ethylene oxide) PEO, has been used as a polymeric host. The reason behind that is, that PEO gains relatively higher electrochemical stability also an exceptionally high ability to complex/dissolve a variety of ionic salts containing larger anions as compared to other polymers. PEO has a mixed semicrystalline/amorphous phase at room temperature. The degree of crystallinity depends upon temperature and the amorphous region increases gradually when the temperature gets increases. The characteristic structure transition on PEO from semicrystalline to amorphous phase is at  $\sim 69$  °C. PEO is a semicrystalline polymer; it contains ether oxygen in its main chain, which coordinates with the cations of the complexed salt and works as a solid solvent. The segmental motion of the polymer chains, in PEO-based electrolytes, is responsible for ion transport, which mainly depends on the amorphous phase of the system [24–26]; unfortunately, the crystalline nature of PEO limits the ionic conductivity of these electrolytes and exhibits low ionic conductivity ( $\sigma_{rt} < 10^{-4}$  S/cm) at room temperature, which limits the practical applications in electrochemical devices. However, for the improvement of the electrochemical properties of such systems, various techniques have been adopted, which can reduce the crystallinity of PEO-based electrolytes and enhance the ionic conductivity at room temperature. The addition of plasticizers is the most common procedure, viz., propylene carbonate (PC), ethylene carbonate (EC), dibutyl phthalate (DBP), dimethyl carbonate (DMC), and diethyl carbonate (DEC) [27–29]. The addition of plasticizers will encourage deterioration of the mechanical properties and increase their reactivity towards the metallic anode. The recent techniques we are using for the increment of ionic

conductivity of solid polymer electrolyte at room temperature is the dispersion of nano-sized inorganic ceramic filler particles, viz.,  $\text{Al}_2\text{O}_3$ ,  $\text{SiO}_2$ ,  $\text{TiO}_2$ ,  $\text{SnO}_2$ ,  $\text{ZnO}$ , and  $\text{ZrO}_2$  into the system [21, 25, 30, 31].

In this manuscript, the binary system of  $\text{NaI-Na}_3\text{PO}_4$  which is already reported by Ahmad et al. in 2014 [32] and also revised in the present study has been complexed with PEO as complexing salt. The reason behind this is iodide systems are the most common solid electrolyte/superionic solids, having very good ionic conductivity, but these are hygroscopic in nature. Alkali phosphate is commonly added to iodide-containing systems to reduce hygroscopicity and improve electrical conductivity [33]. Polymer electrolyte samples have been prepared by a novel hot-press method, which is a more rapid, cost-effective, completely dry/solvent-free, and less time-consuming method as compare to the conventional solution cast method [34–37]. In the present investigation,  $\text{Na}^+$ -conducting nano-composite polymer electrolyte (NCPE) membranes, (70PEO: 30 [50NaI + 50 $\text{Na}_3\text{PO}_4$ ] +  $y$  ZnO), in varying filler concentration ( $y$ ) have been synthesized using SPE film composition, (70PEO: 30 [50NaI + 50 $\text{Na}_3\text{PO}_4$ ]), as 1st-phase host matrix and ZnO nano-filler as 2nd-phase dispersoid from filler particle concentration-dependent conductivity measurements on different NCPE films. Organic fillers are more expensive than inorganic fillers; hence we employed inorganic filler (ZnO) in our study, and ZnO is a metallic oxide that is also used to improve the chemical stability of the electrolyte system [38, 39]. Optimum conducting composition (OCC) NCPE film has further been identified and subjected to various characterization studies, viz., ion transport/structural/thermal properties in order to evaluate its applicability in potential all-solid-state electrochemical devices, viz., batteries.

## Experimental section

### Materials

AR grade precursor chemicals, poly (ethylene oxide) PEO ( $6 \times 10^5$  Mw, purity > 99%, Aldrich, USA), NaI (99%, Loba chemie, India),  $\text{Na}_3\text{PO}_4$  (99%, Loba chemie, India), and ZnO nano-powder (< 100 nm, Aldrich, USA), were used as received.

### Preparation of SPE and NCPE film membrane

The electrolyte membranes have been prepared by a novel solvent-free/dry hot-press technique. NCPE films, (70PEO: 30 [50NaI + 50 $\text{Na}_3\text{PO}_4$ ] +  $y$  ZnO), in varying filler concentrations, viz.,  $y = 0, 1, 2, 3, 4, 5$ , and 6 wt. (%), have been synthesized. Based on a composition-dependent

conductivity study, an SPE composition of (70PEO: 30 [50NaI + 50Na<sub>3</sub>PO<sub>4</sub>]), 70:30 wt. (%), was identified as the optimum conducting composition (OCC) and was chosen as a polymer electrolyte host for dispersal of nano-sized ZnO particles to prepare nano-composite polymer electrolyte (NCPE) membranes. All the precursor chemicals were under vacuum dried (Meta-Lab vacuum oven, India), PEO at 50 °C and remaining at 100 °C for overnight, and the dry powders of SPE film composition, (70PEO: 30 [50NaI + 50Na<sub>3</sub>PO<sub>4</sub>]), were selected as 1st-phase host and ZnO in different wt. (%) ratios as 2nd-phase were mixed physically for ~45 min by an agate mortar pestle. The physically mixed, homogeneous mixture was heated close to the melting/softening point of PEO, i.e., ~70 °C, and applied hot mixing for ~30 min continued. As a result, a soft lump/slurry is obtained, and then it is pressed (~1–2 ton/cm<sup>2</sup>) between two pre-heated stainless steel (SS) blocks by KBr press machine (Techno Search Instruments Ltd., India) which give rise to a uniform and flexible thin film of thickness on the order of ~100–200 μm and placed in vacuum-sealed desiccator.

## Material characterization

The structural property studies have been performed by X-ray diffraction (XRD) analysis. Using a Siemens diffractometer and Cu-Kα radiation (D2 phaser model: 08 discover, Bruker, Germany; Cu-Kα radiation: λ = 1.54 Å), the XRD data were obtained from thin-film samples at room temperature. XRD patterns were collected with 2θ varying from 10° to 60°. The surface morphological study was analyzed using an SEM (JSM-IT300, In TouchScope™ Scanning Electron Microscope) and energy-dispersive spectroscopy (EDS or EDAX) (Ametek EDS system).

The thermal properties of synthesized SPE host and NCPE OCC film were characterized by thermogravimetric analyzer (TGA) (STARE SYSTEM TGA1 SF/1100) and differential scanning calorimetry (DSC) (STARe, SW 13.00, METTLER) techniques. From the TGA plot, the thermal stability of the sample can be observed, and by DSC thermograms, the degree of crystallinity ( $X_c$ ) can be studied with the help of the following equation [40]:

$$X_c = \left( \frac{\Delta H_m}{\Delta H_m^0} \right) \times 100\% \quad (1)$$

where  $\Delta H_m$  is the melting enthalpy estimated experimentally from the peak area and  $\Delta H_m^0$  (~213.7 J g<sup>-1</sup>) is the literature value of melting enthalpy for 100% crystalline PEO [41].

The bulk resistance ( $R_b$ ) of the polymer electrolyte film has been obtained by the complex impedance plot (Nyquist plot). In the complex impedance spectroscopy method, the SPE and NCPE films were sandwiched between two

stainless steel electrodes, i.e., SS||SPE/NCPE||SS, and the frequency-dependent impedance data was obtained by LCR meter [42]. The graph depicts two arcs, one at a lower frequency region and the other at a higher frequency region. The electrode–electrolyte interface phenomenon is linked to the low-frequency arc and the arc at the higher frequency region contains data on bulk phenomena, particularly ion conduction. The capacitive nature is demonstrated by the low-frequency arc [43, 44]. The bulk resistance corresponding to the minima in the imaginary part of impedance ( $Z''$ ) is extracted using the dip in the figure. With the addition of salt, the dip becomes more frequent and indistinct.

Ionic conductivity measurements were performed by impedance spectroscopy (IS) method with varying the frequency in the range of 1 mHz–200 kHz using an LCR meter (HIOKI IM 3533, Japan). In this study, the ionic conductivity is calculated by the following equation [25]:

$$\sigma = \frac{d}{R_b A} \quad (2)$$

where " $R_b$ " is the bulk resistance (Siemens<sup>-1</sup>, S<sup>-1</sup>), " $d$ " is the thickness (cm), and " $A$ " is the known cross-sectional area of the electrolyte–electrode (cm<sup>2</sup>). The temperature-dependent conductivity measurement was performed on SPE host and NCPE OCC films to understand the ion-transport mechanism and calculate activation energy ( $E_a$ ) by linear least square fitting method of " $\log \sigma - 1/T$ " Arrhenius plot.  $E_a$  is calculated by the following equation:

$$\log \sigma = \log \sigma_0 - \frac{E_a}{KT} \quad (3)$$

In the above equation " $\sigma_0$ " is the pre-exponential factor, " $K$ " represents the Boltzmann constant, and " $E_a$ " is the activation energy. The total ionic transference number ( $t_{ion}$ ) of NCPE OCC film was calculated by the dc polarization Transient Ionic Current (TIC) method. The film sample was kept between SS (stainless steel) (blocking) electrodes, was subjected to a constant dc polarizing potential (V) ~1 V, and the variation in current is monitored as a function of time.  $t_{ion}$  was calculated from

$$t_{ion} = \frac{I_{ion}}{I_T} \quad (4)$$

obtained from the "current vs time" TIC plot.

Also, dielectric behavior has been studied for prepared NCPE OCC membranes. The complex dielectric behavior of a polymeric sample is illustrated as

$$\epsilon^* = \epsilon' - i\epsilon''$$

where  $\epsilon'$  and  $\epsilon''$  are the real and imaginary parts of dielectric constant, respectively, and these dielectric constants can be given by the following equation [45, 46]:

$$\epsilon' = \frac{C_p d}{\epsilon_0 A} \quad (5)$$

$$\epsilon'' = \frac{\sigma}{\omega \epsilon_0} \quad (6)$$

where “ $C_p$ ” is the parallel capacitance, “ $d$ ” is the thickness of the polymeric electrolyte film, “ $\epsilon_0$ ” is the permittivity of free space, “ $\sigma$ ” is the ionic conductivity of the polymer electrolyte, and “ $\omega$ ” is the angular frequency, where  $\omega = 2\pi f$  presents the frequency in Hertz (Hz). The frequency range is 1 mHz to 200 kHz, over the temperature region from 303 to 373 K.

## Results and discussions

Figure 1a shows the XRD patterns of the various polymer electrolyte membranes. In XRD of pure PEO, two major peaks have been observed at Bragg’s angles  $2\theta \sim 19.3^\circ$  and  $\sim 23.3^\circ$ , respectively. It exhibits the semicrystalline nature of pure PEO. After the complexation of the sodium binary system, no peaks of the sodium binary system have been observed separately in the diffractogram, which suggests that the salt is completely dissociated and is consistent with prior research [47]. However, it is clearly observed that the intensity of the peaks is reduced with the complexation of the sodium binary system; also with the dispersion of ZnO nano-filler particles, the intensity of two main peaks of PEO got suppressed significantly [25, 48, 49] and some small additional peaks are observed due to ZnO which can be confirmed by XRD of pure ZnO. Figure 1b shows the XRD patterns with expanded regions: (a) pure PEO, (b) SPE host film, and (c) NCPE OCC film, and also exhibits the shifting and the splitting of the XRD crystalline peaks, which points towards the formation of a new crystalline ordering in the polymer electrolytes occurs due to the complexation of binary sodium system and ZnO nano-filler. In SPE host and NCPE OCC films, the reduction in the XRD peak’s intensity is due to the destruction of crystalline phases [24]. The addition of a binary sodium system and dispersion of ZnO nano-particles may be responsible for creating polycrystalline phases. These types of solids are made up of numerous small grains. The grains are separated by grain boundaries, which have random crystallographic orientations and serve as pathways between grains. Due to the small grain size, the activation energy ( $E_a$ ) (which is the minimum required energy for ion hopping) should also be reduced, which supports the easily ion migration and enhancement of ionic conductivity [50, 51]. Also, the SEM (Fig. 2a, c) and DSC study (Table 2) support a reduction in the degree of crystallinity for SPE host and NCPE OCC film in comparison with pure PEO.

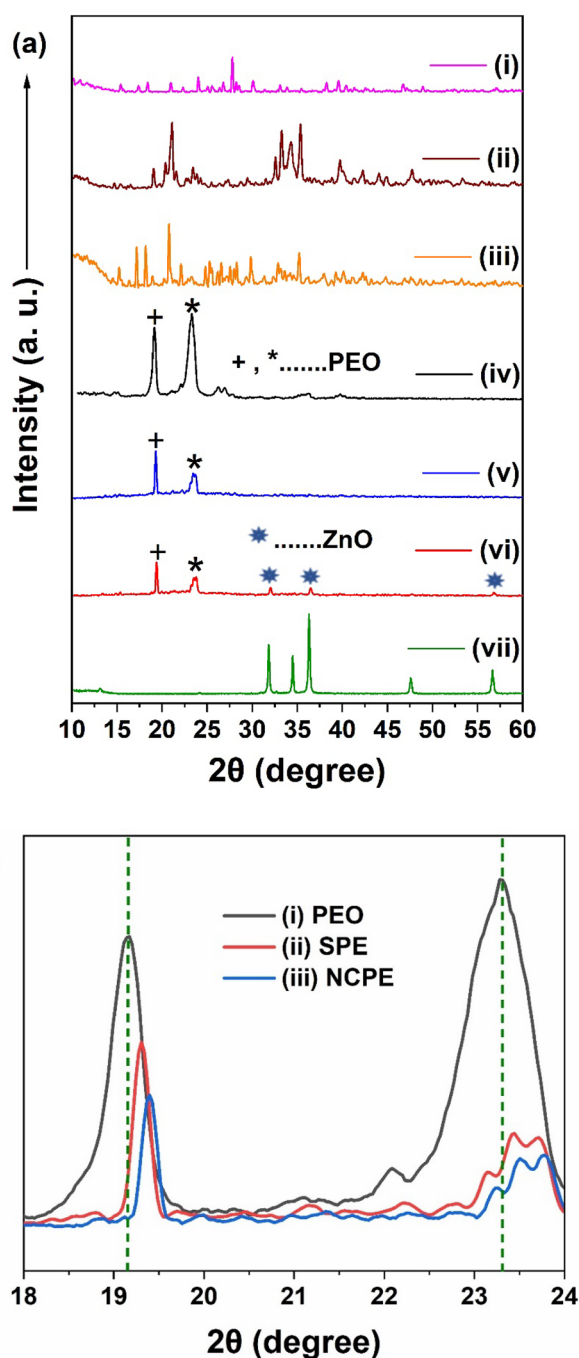
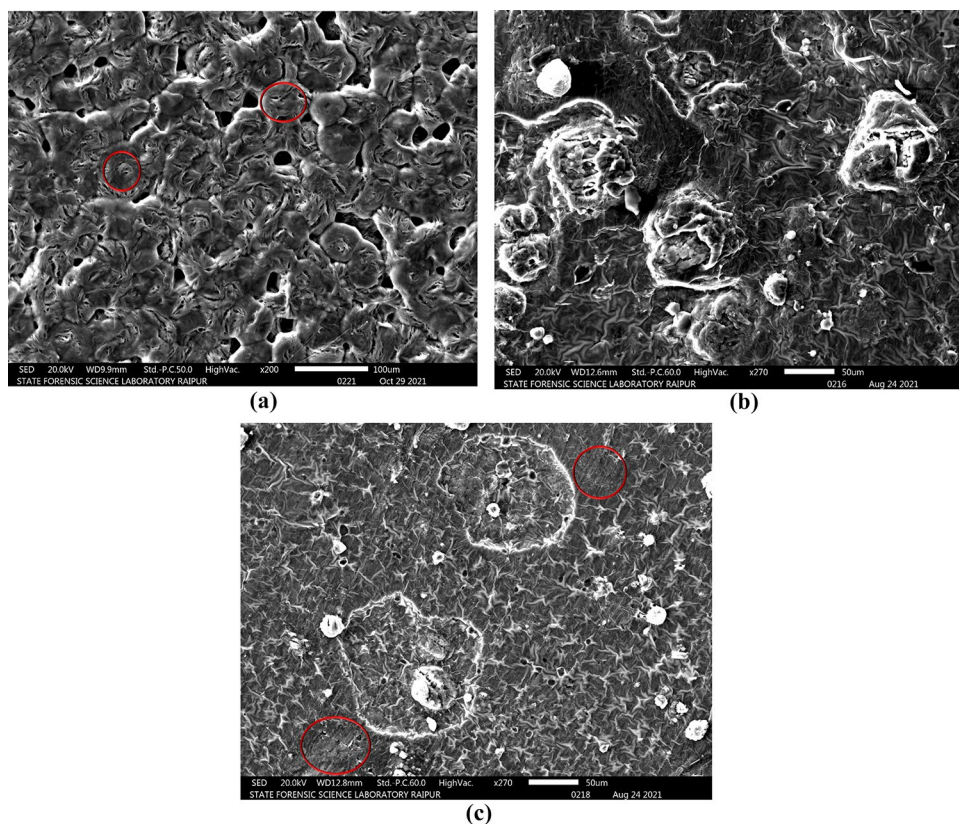


**Fig. 1** **a** XRD pattern for (i) NaI salt, (ii)  $\text{Na}_3\text{PO}_4$  salt, (iii) composite: (50NaI: 50 $\text{Na}_3\text{PO}_4$ ), (iv) pure PEO, (v) SPE host: (70PEO: 30 [50NaI+50 $\text{Na}_3\text{PO}_4$ ]) film, (vi) NCPE OCC: (70PEO: 30 [50NaI+50 $\text{Na}_3\text{PO}_4$ ]+4 ZnO) film, and (vii) pure ZnO filler. **b** XRD pattern with expanded regions: (i) pure PEO, (ii) SPE host film, and (iii) NCPE OCC film

Figure 2 shows the SEM images of the surfaces of pure PEO, SPE host, and NCPE OCC films. The ionic conductivity of the electrolyte is affected by the surface morphology as well as with crystallinity of the polymer electrolyte



**Fig. 2** SEM images of **a** pure PEO, **b** SPE host film, and **c** NCPE OCC film



membrane. Polymer electrolytes with smooth surfaces exhibit superior ionic conductivity [52]. In the pure PEO film, the rough morphology of compact spherulitic structures is observed, and the spherulite structure indicates the semicrystalline nature of pure PEO (spherulitic structure marked in Fig. 2a). Binary system of NaI-Na<sub>3</sub>PO<sub>4</sub>, which SEM image already reported [32], complexed with PEO with 30 wt. (%); the size of the spherulites has been reduced, which means crystalline nature of the PEO decreases. The surface morphology of the polymer-salt matrix evolving from rough to smooth after the addition of ZnO nano-filler suggested that the filler is dispersed uniformly throughout the polymer-salt matrix (smooth surface morphology marked in Fig. 2c). Spherulites have been reduced significantly, which confirms the enhancement of the amorphous phase in the polymer electrolyte films, as observed in XRD as well DSC thermograms. It is clear from the figure that with 4 wt. (%) of ZnO, the surface becomes significantly smooth with few cracks, confirming that a gradual increase in the amorphous phase supports the fast ion transportation in the polymer electrolyte system [52, 53]. Furthermore, by rolling the film, the flexibility of the thin film is demonstrated in Fig. 3a, b.

Figure 4 shows the EDAX and element mapping of the pure PEO, SPE host, and NCPE OCC film. The existence of all key elements in the prepared system is confirmed

by the EDAX spectrum. Carbon (C), oxygen (O), sodium (Na), phosphorus (P), iodine (I), and zinc (Zn) elements are clearly visible without any substantial contaminants. The obtained results indicate a uniform (70PEO: 30 [50NaI + 50Na<sub>3</sub>PO<sub>4</sub>] + 4 ZnO) film formation.

Figure 5 shows the thermogravimetric (TG) curves of the pure PEO, SPE host, and NCPE OCC films. The dynamic thermogravimetry investigation, for the weight loss of the samples as a function of temperature, was performed under a nitrogen atmosphere in the temperature range of 25–600 °C

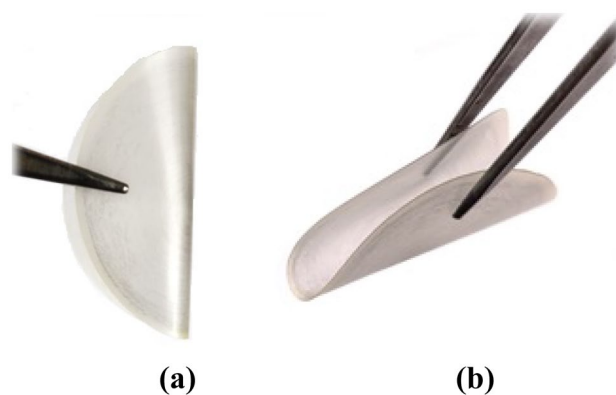
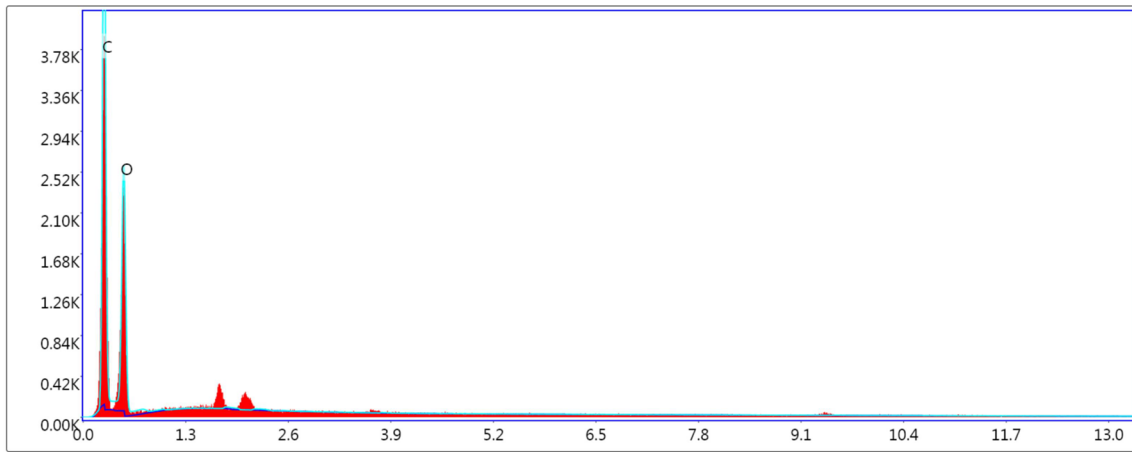
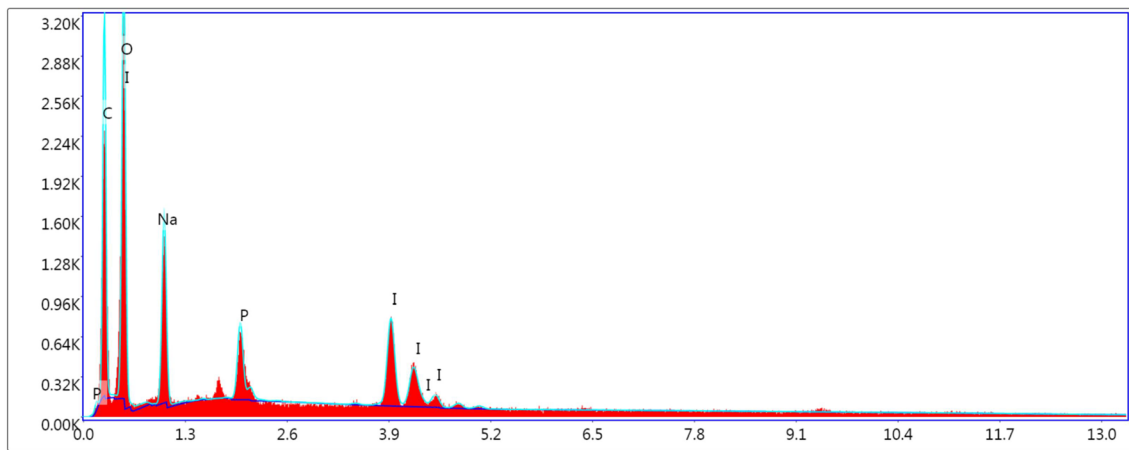


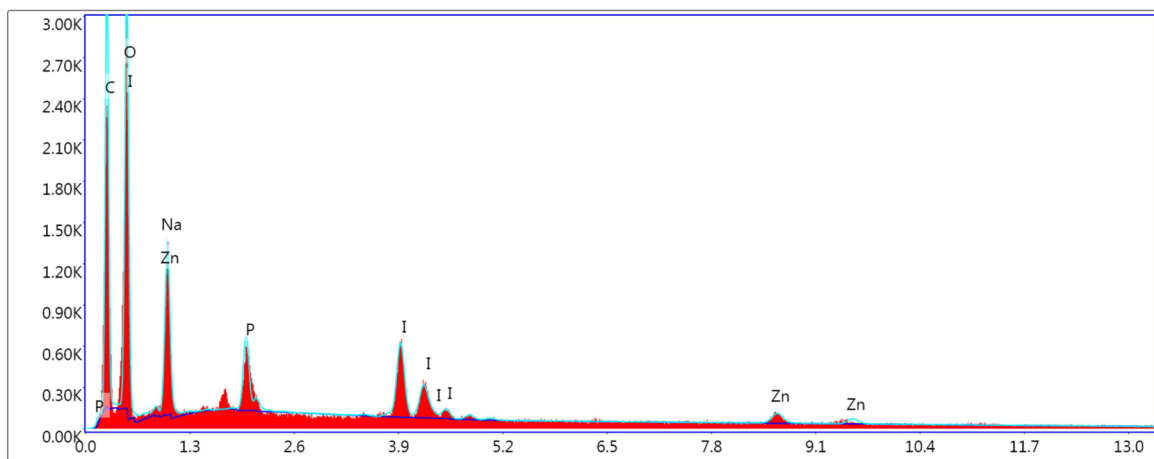
**Fig. 3** Digital photograph of prepared films: **a** and **b** films are flexible



(a)



(b)



(c)

**Fig. 4** EDAX spectrum of **a** pure PEO, **b** SPE host film, and **c** NCPE OCC film

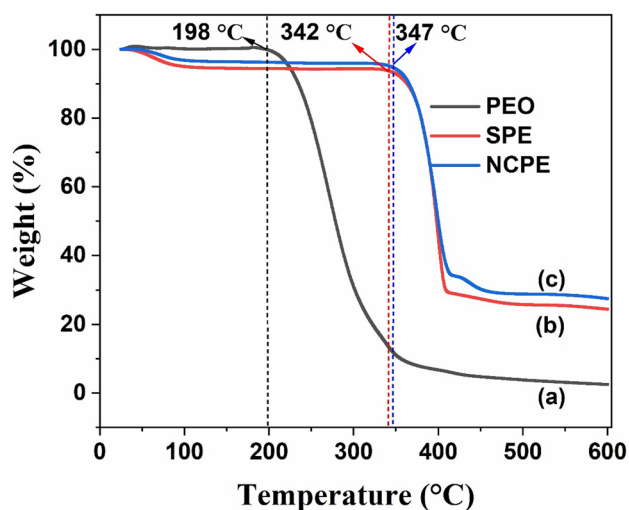


**Fig. 5** TGA traces of **a** pure PEO, **b** SPE host film, and **c** NCPE OCC film

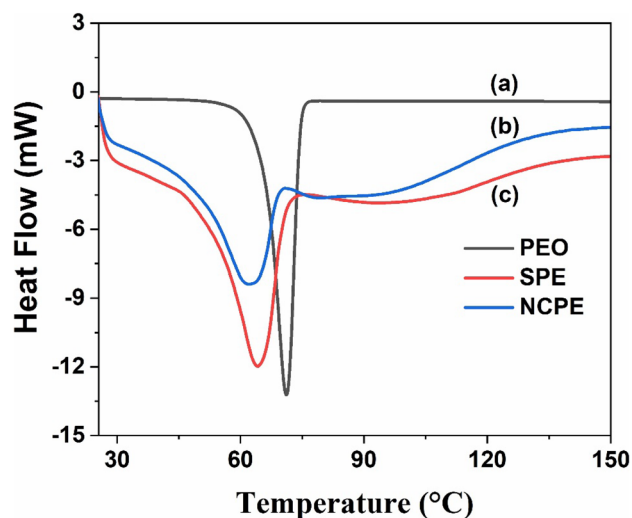
[47]. The TGA curves of the PEO, SPE host, and NCPE OCC films present the three major weight loss regions:

- The first region is at a temperature below 100 °C. At this temperature range weight loss has been observed for all samples due to the evaporation of absorbed moisture.
- The second region of around 200 °C PEO starts irreversible degradation and is due to the decomposition of weak poly (ethylene oxide) chains and no remarkable weight loss is observed after 400 °C for pure PEO [46].
- The third region of around 350–450 °C is due to the decomposition of the PEO-salt-filler membrane.

Based on the keen observation of TGA curves and from Table 1, it is clear that by the complexation of salt and dispersion of filler particles, the thermal stability of polymer membrane increases up to ~350 °C and the mass loss ( $\Delta m$ ) decreases [25]. The thermal stability of SPE and NCPE films got enhanced due to the shielding effect provided by the binary sodium system and ZnO nano-particles, which provides a remarkable barrier effect to the polymer electrolyte from thermal degradation [54].

**Table 1** The percentage values of weight loss of pure PEO, SPE host film, and NCPE OCC film at different temperatures

Sample	Weight loss %				
	100 °C	200 °C	300 °C	400 °C	500 °C
Pure PEO	0.26	0.39	69.09	93.16	96.25
SPE OCC	5.29	5.48	5.69	52.59	74.18
NCPE OCC	3.28	3.69	4.06	50.31	71.09



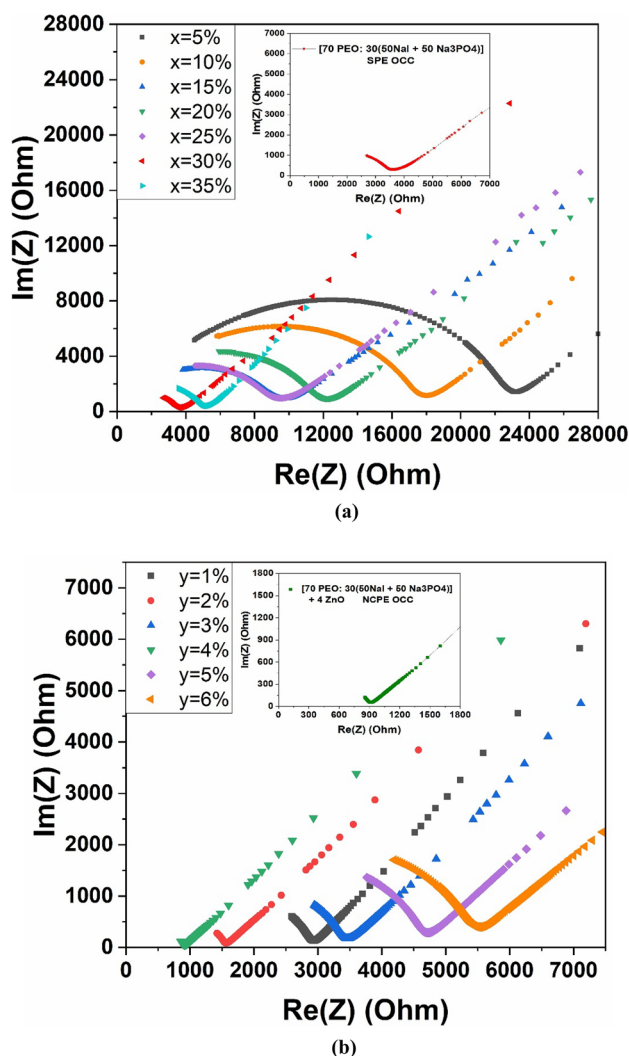
**Fig. 6** Differential scanning calorimetry curves of **a** pure PEO, **b** host film, and **c** NCPE OCC film

Figure 6 shows that the DSC curves for the pure PEO; SPE host, (70PEO: 30 [50NaI + 50Na<sub>3</sub>PO<sub>4</sub>]); and NCPE OCC, (70PEO: 30 [50NaI + 50Na<sub>3</sub>PO<sub>4</sub>]) + 4ZnO films, over the temperature range of 25 to 150 °C were performed under a nitrogen atmosphere. It can be clearly seen that the sharp endothermic peaks at the melting temperatures of the films have been presented, and in the case of the SPE host and NCPE OCC, the degree of crystallinity ( $X_c$ ), which is calculated using Eq. (1), and the melting enthalpy ( $\Delta H_m$ ) are both reducing. It may be noted from Table 2 that the melting temperature ( $T_m$ ) is located at 71.09 °C for pure PEO and slightly shifted towards a lower temperature region for both the SPE host and NCPE OCC films. The shifting of endothermic peaks is due to the complexation of the binary sodium system and the dispersion of ZnO nano-filler in the polymer network. In PEO-based solid polymer electrolytes, sodium-ion conduction increases in the amorphous phase in comparison to the crystalline phase, which is also in perfect agreement with the XRD, A.C. impedance spectroscopy (IS) study [47, 55].

Figure 7 shows the Nyquist plot for SPE and NCPE films, which shows the imaginary component ( $Z''$ ) vs the real part ( $Z'$ ). The ionic conductivities of solid polymer electrolyte (SPE) and nano-composite polymer electrolyte (NCPE) films

**Table 2** The values of  $T_m$ ,  $\Delta H_m$ , and  $X_c$  for pure PEO, SPE host film, and NCPE OCC film

Film sample	$T_m$ (°C)	$H_m$ (J/g)	$X_c$ (%)
Pure PEO	71.09	175.15	81.90
SPE OCC	64.26	68.57	32.09
NCPE OCC	62.25	53.05	24.82



**Fig. 7** **a** Nyquist plots of SS||SPE host||SS with different concentrations of  $(1-x)$  PEO:  $x$  ( $50\text{NaI} + 50\text{Na}_3\text{PO}_4$ ), where  $x = 5, 10, 15, 20, 25, 30,$  and  $35$  wt. (%). **b** Nyquist plots of SS||NCPE OCC||SS with different concentrations of  $(70\text{PEO}: 30[50\text{NaI} + 50\text{Na}_3\text{PO}_4]) + y$  ( $\text{ZnO}$ ), where  $y = 1, 2, 3, 4, 5,$  and  $6$  wt. (%)

are calculated using Eq. (2), and the bulk resistance “ $R_b$ ” is obtained from the Nyquist plot. Figure 7a shows the obtained ionic conductivities of solid polymer electrolytes  $(1-x)$  PEO:  $x$  ( $50\text{NaI} + 50\text{Na}_3\text{PO}_4$ ) for the different concentrations of binary sodium system ( $50\text{NaI}: 50\text{Na}_3\text{PO}_4$ ), where  $x = 5, 10, 15, 20, 25, 30,$  and  $35$  wt. (%), and Fig. 7b represents the NCPE ( $70\text{PEO}: 30 [50\text{NaI} + 50\text{Na}_3\text{PO}_4] + y$  ( $\text{ZnO}$ ), where  $y = 1, 2, 3, 4, 5,$  and  $6$  wt. (%). It is clear that when the concentration of the binary sodium system ( $50\text{NaI}: 50\text{Na}_3\text{PO}_4$ ) is increased, the ionic conductivity increases. The maximum ionic conductivity ( $\sigma_{rt}$ )  $\sim 4.89 \times 10^{-6}$  S/cm is obtained at room temperature for  $(70\text{PEO}: 30 [50\text{NaI} + 50\text{Na}_3\text{PO}_4])$  confirms as SPE host film. However, by the dispersion of ZnO as 2nd-phase insulating nano-particles/passive filler into the 1st-phase SPE host matrix, an ionic conductivity increases by approximately an order of magnitude, which exhibits the room temperature conductivity ( $\sigma_{rt}$ )  $\sim 1.45 \times 10^{-5}$  S/cm (Table 3) for the composition of  $(70\text{PEO}: 30 [50\text{NaI} + 50\text{Na}_3\text{PO}_4]) + 4\text{ZnO}$ . The addition of filler particles may facilitate ionic transport and polymer segmental mobility, increasing conductivity [56]. Table 4 compares the ionic conductivity values, reported in the literature with other polymer electrolyte systems. The conductivity enhancement can also be explained in two ways based on the changes in XRD patterns and DSC results. Firstly, in the PEO-ZnO-binary sodium system, crosslinking reduces the crystallinity of the films, resulting in more amorphous regions being available for transporting the charge carriers. In another way, the combined effects of PEO and ZnO nano-particles break the binary sodium system into ion pairs, releasing more free cations and anions in the polymer electrolyte, which are the free charge carriers [57]. The ionic conductivity of a polymer electrolyte membrane containing multiple ionic species can also be given by  $\sigma = nq\mu$ , and the composition-dependent conductivity of polymer electrolytes can vary due to the number of charge carriers ( $n$ ), ion mobility ( $\mu$ ), or both. The low activation energy value (Table 3) with the enhanced amorphous phase confirms faster ion migration which supports the faster segmental motion of polymer chains. It is clear that the overall increase in ionic conductivity of NCPE OCC is the result of a moderate increase in mobility ( $\mu$ ) and/or

**Table 3** The values of  $\sigma_{rt}$ ,  $t_{ion}$ , and  $E_a$  for SPE host and NCPE OCC films along with  $\sigma_{rt}$  of pure PEO

Film sample	$\sigma_{rt}$ (S/cm)	$t_{ion}$	$E_a$ (eV)
Pure PEO	$3.2 \times 10^{-9}$	-	-
SPE OCC: (70PEO: 30 [50NaI + 50Na <sub>3</sub> PO <sub>4</sub> ])	$4.89 \times 10^{-6}$	0.99	0.39
(70PEO: 30 [50NaI + 50Na <sub>3</sub> PO <sub>4</sub> ]) + 1ZnO	$4.87 \times 10^{-6}$	-	-
(70PEO: 30 [50NaI + 50Na <sub>3</sub> PO <sub>4</sub> ]) + 2ZnO	$9.64 \times 10^{-6}$	-	-
(70PEO: 30 [50NaI + 50Na <sub>3</sub> PO <sub>4</sub> ]) + 3ZnO	$4.62 \times 10^{-6}$	-	-
NCPE OCC: (70PEO: 30 [50NaI + 50Na <sub>3</sub> PO <sub>4</sub> ]) + 4ZnO	$1.45 \times 10^{-5}$	0.99	0.35
(70PEO: 30 [50NaI + 50Na <sub>3</sub> PO <sub>4</sub> ]) + 5ZnO	$3.55 \times 10^{-6}$	-	-
(70PEO: 30 [50NaI + 50Na <sub>3</sub> PO <sub>4</sub> ]) + 6ZnO	$2.89 \times 10^{-6}$	-	-



**Table 4** The value of ionic conductivities for different ceramic nano-filler-based nano-composite polymer electrolyte membranes

Film sample	Conductivity	Temperature (°C)	Reference
PEO–LiClO <sub>4</sub> –10% ZnO	$1.28 \times 10^{-5}$	35	[39]
PEO–NaPF <sub>6</sub> –5% ZrO <sub>2</sub>	$2.80 \times 10^{-6}$	40	[68]
PEO–Cu(ClO <sub>4</sub> ) <sub>2</sub> ·6H <sub>2</sub> O–2% Al <sub>2</sub> O <sub>3</sub>	$1.76 \times 10^{-5}$	RT	[25]
PEO–LiClO <sub>4</sub> –10% SiO <sub>2</sub>	$2.30 \times 10^{-5}$	25	[69]
PEO–AgNO <sub>3</sub> –10% TiO <sub>2</sub>	$1.10 \times 10^{-6}$	RT	[31]
<b>(70PEO: 30 [50NaI + 50Na<sub>3</sub>PO<sub>4</sub>]) + 4 ZnO</b>	<b><math>1.45 \times 10^{-5}</math></b>	<b>RT</b>	<b>Present study</b>

RT room temperature

number of charge carriers ( $n$ ) [58]. However, excess filler concentration in the solid polymer electrolyte may lead to ion pairs and ion aggregation, which blocks ionic conduction and decreases ion mobility ( $\mu$ ), in an amorphous phase, which could explain the decrease in ionic conductivity with increasing filler concentration. In the case of NCPE films for 2 wt. (%) ZnO, a modest increase in ionic conductivity is noticed before. The existence of two conductivity maxima has been reported earlier in various composite and nano-composite polymer electrolytes and has been explained by two percolation models suggested by Lakshmi and Chandra [59]. It has been suggested that the two types of conductivity maxima are caused by transport mechanisms in these systems. The first maxima, according to this model, are caused by the dissociation of ion aggregates and/or un-dissociated salt, resulting in the formation of free ion carriers as a result of the addition of nano-sized ZnO particles. The second conductivity maxima are linked to the well-known two-phase composite phenomenon, which may be explained using a space charge and/or percolation model [60].

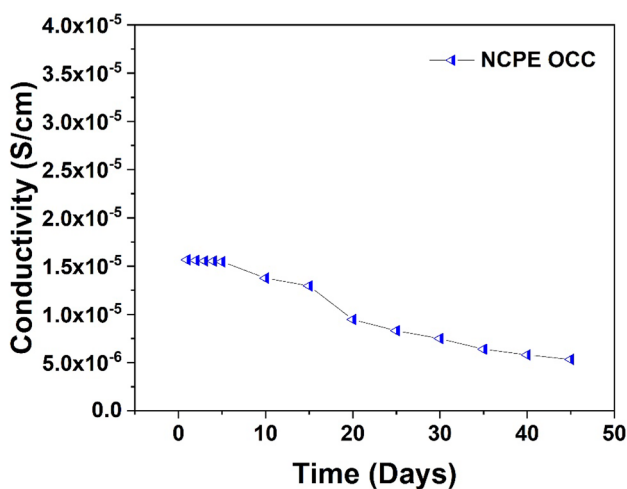
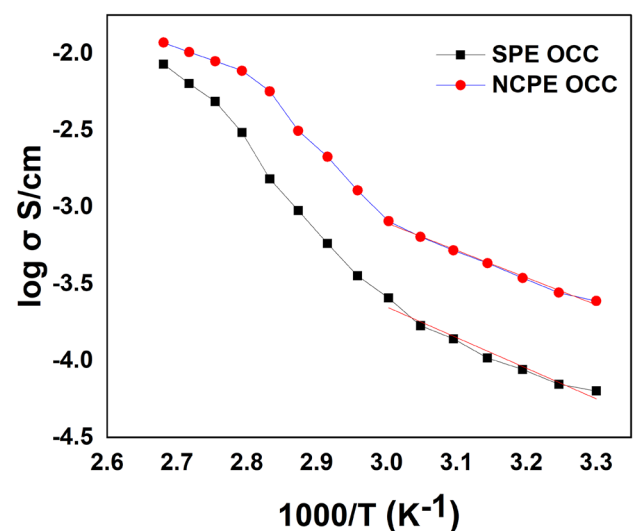
**Fig. 8** Time-dependent room temperature conductivity study for NCPE OCC film

Figure 8 shows time-dependent conductivity study on NCPE OCC membrane at room temperature ( $\sigma_{rt} \sim 1.45 \times 10^{-5}$  S/cm). It is well known that the re-crystallization process of host polymer PEO-based electrolytes can result in a decrease in conductivities, limiting the use of PEO for solid-state batteries, particularly at room temperature [61]. However, the conductivity of the NCPE OCC membrane remains stable for 15 days and then starts gradually decaying from  $10^{-5}$  to  $10^{-6}$  S/cm after 3 weeks.

Figure 9 shows the temperature-dependent conductivity studies by Arrhenius plot between “ $\log \sigma - 1000/T$ ” for SPE host and NCPE OCC films in the temperature range of 303 to 373 K. Conductivity increases linearly with temperature, exhibiting Arrhenius-like behavior. Increased ionic conductivity is caused by a decrease in polymer viscosity and as a result, a rise in polymer flexibility. Thermal activation of charge carriers facilitates cation migration to the next coordinating site, while increased free volume promotes ion migration. It is obvious from both plots that conductivity rose linearly at first, then a minor upward change in slope,

**Fig. 9** Arrhenius plot for SPE host and NCPE OCC film as a function of the various temperatures

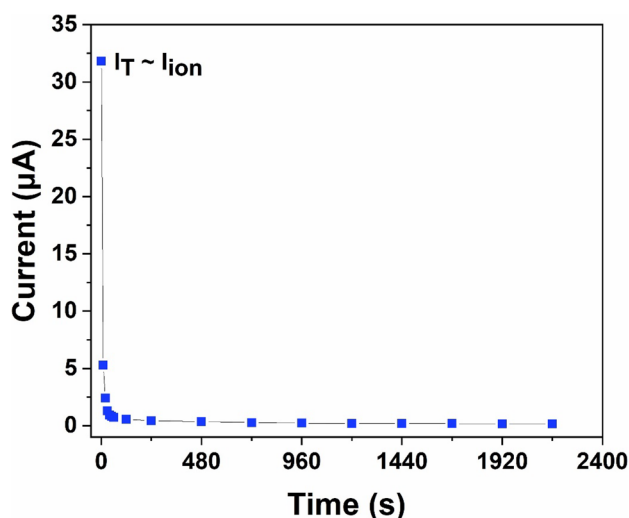


Fig. 10 “Current–time” TIC plot for NCPE OCC film

which corresponds to the normal semi-crystalline to completely amorphous phase transition of pure polymer PEO, and that the conductivity became saturated at higher temperatures. It also suggested that the amorphous phase be enhanced, as this is a necessary condition for a solid-state ionic conductor. The activation energy ( $E_a$ ) was calculated using the Arrhenius straight-line equation, and the least square fitting of the linear component of the “ $\log \sigma - 1000/T$ ” plot using Eq. (3).  $E_a$  was computed at the lower temperature region of the  $\log \sigma - 1000/T$  plot and found to be  $\sim 0.35$  eV for NCPE (Table 3).

There could be several mobile species in the ion-conducting solids and there are free electrons in the system; they will participate in the conduction process as well. As a result, it is crucial to figure out whether the conductivity of the sample is caused by ions, electrons, or holes. If the conductivity of the system is only owing due to ions, the system is purely ionic, and the value of  $t_{\text{ion}} \sim 1$  is obtained by the dc polarization TIC technique described in the “Experimental section”; the total ionic transport number  $t_{\text{ion}}$  on the nano-composite polymer electrolyte (70PEO: 30[50NaI + 50Na<sub>3</sub>PO<sub>4</sub>] + 4 ZnO) was also determined. The variation of current as a function of time when a dc voltage of 1 V is applied across the

cell SS||NCPE||SS (SS: stainless steel) is shown in Fig. 10. Equation (4) was used to calculate the value of  $t_{\text{ion}}$ , which was calculated to be  $\sim 0.99$  (Table 3). Based on the variance of current and the degree of transport number, the overall conductivity is primarily ionic. It means that ions are responsible for the majority of carrier transport and that electrons are playing a minor role. It signifies that those ions are the majority of carrier transport while electrons are only involved in a minor way.

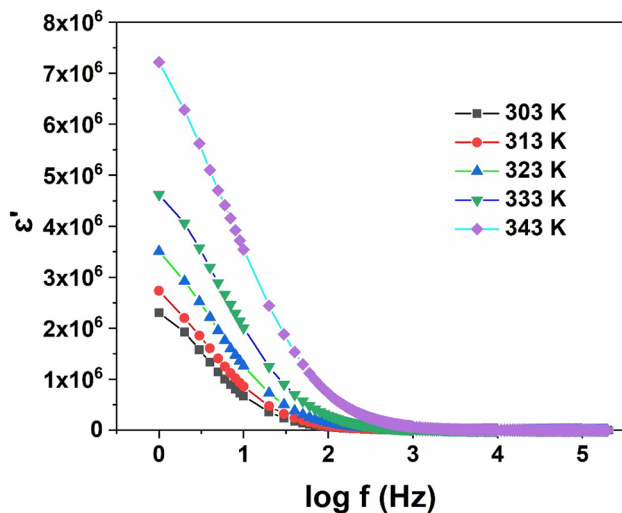
The variation of dielectric constant and dielectric loss versus temperature is different for non-polar and polar polymers. Basically, dielectric constant and dielectric loss both are independent of temperature for the non-polar types of polymers, but in the case of polar polymers like PEO [62], the dielectric constant, as well as dielectric loss, increases along with the increasing temperature as mentioned in Table 5. This behavior can be ascribed to the fact that the orientation of dipoles was facilitated by the temperature rise and thus, permittivity increased [63]. Dielectric constant and dielectric loss have been calculated using Eqs. (5) and (6).

Figure 11 shows the plot between  $\epsilon'$  vs  $\log f$  (Hz) of NCPE OCC film in the different temperature ranges. On clear observation, it has been found that the NCPE film shows the characteristics in which the dielectric constant decreases at a higher frequency region and increases at a lower frequency region. The enhancement of  $\epsilon'$  at lower frequency region is due to the alignment of dipoles together with the ionic and space charge polarization in the direction of the electric field, which is typical behavior of dielectrics; the dipole alignment becomes clear with raising the temperature. However, at higher frequency regions, discrete dipoles are no longer able to align sufficiently in the direction of the applied electric field; hence, their oscillation begins to lag, and the dielectric constant starts to decrease. This behavior is supported by the experimental result;  $\epsilon'$  increases with lowering the frequency, and the same results are also observable when the temperature increases. In this study,  $\epsilon'$  is increased with temperature due to an increment in the number of charge carriers resulting from the segregation of ion aggregates [31].

Figure 12 shows the plot between  $\epsilon''$  vs  $\log f$  (Hz) of NCPE OCC film in the different temperature ranges; it

**Table 5** Values of dielectric constant and dielectric loss in different frequencies

Temperature (K)	Dielectric constant				Dielectric loss			
	1 Hz	100 Hz	1 kHz	200 kHz	1 Hz	100 Hz	1 kHz	200 kHz
303	$2.30 \times 10^6$	$6.55 \times 10^4$	$4.12 \times 10^3$	$2.11 \times 10^1$	$4.63 \times 10^4$	$2.27 \times 10^3$	$2.75 \times 10^2$	$1.64 \times 10^0$
313	$2.73 \times 10^6$	$9.14 \times 10^4$	$6.00 \times 10^3$	$2.24 \times 10^1$	$5.54 \times 10^4$	$2.95 \times 10^3$	$3.64 \times 10^2$	$2.19 \times 10^0$
323	$3.50 \times 10^6$	$1.50 \times 10^5$	$1.05 \times 10^4$	$2.55 \times 10^1$	$7.19 \times 10^4$	$4.44 \times 10^3$	$5.59 \times 10^2$	$3.39 \times 10^0$
333	$4.62 \times 10^6$	$2.92 \times 10^5$	$2.29 \times 10^4$	$3.47 \times 10^1$	$9.58 \times 10^4$	$7.63 \times 10^3$	$1.00 \times 10^3$	$6.31 \times 10^0$
343	$7.22 \times 10^6$	$7.23 \times 10^5$	$6.94 \times 10^4$	$5.96 \times 10^1$	$1.51 \times 10^5$	$1.60 \times 10^4$	$2.31 \times 10^3$	$1.52 \times 10^1$



**Fig. 11** The dielectric constant of NCPE OCC film at different room temperatures

is indicated that the reduction of the ion diffusion in the polymer matrix is observed, and ion diffusion occurs due to the rapid change of the applied electric field [64]. Similarly, same as the dielectric constant  $\epsilon'$ , the dielectric loss  $\epsilon''$  starts to decrease when frequency starts to increase; it attains higher values at lower frequencies. Dielectric loss is decreasing with increasing frequency just because of the DC conductivity of the materials. The charge collection at the electrode–electrolyte interface also can increase the dielectric loss at low frequency [48, 65]. The reason behind this, at the lower frequency region sufficient time, is available for the dipole to build up the interface before the alteration of the electric field, which provides a large apparent value of

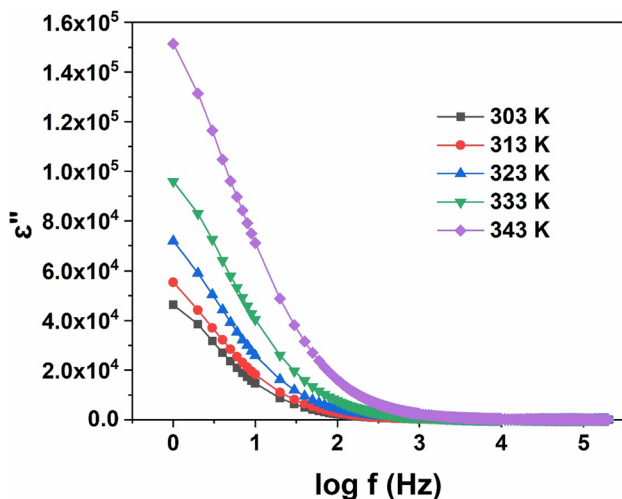


**Fig. 12** The dielectric loss of NCPE OCC film at different room temperatures

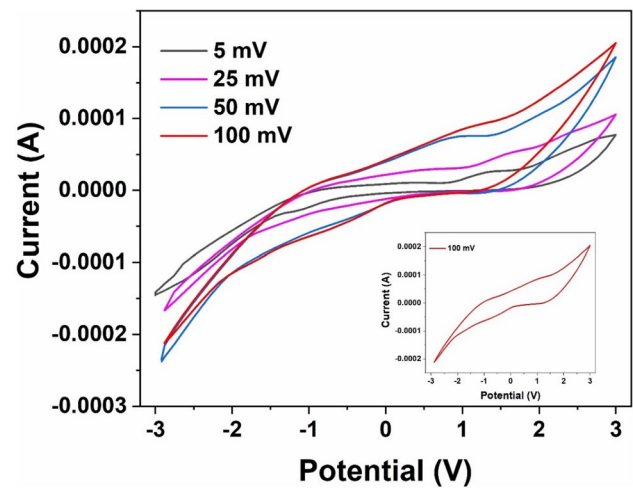


**Fig. 13** Cyclic voltammetry of symmetry cell SSI|NCPE OCC||SS

$\epsilon''$ . However, the frequency is increasing; there is not enough time for the build-up of dipoles at the interface which occurs at the boundaries of conducting species in the materials and at the ends of conducting paths. The enhancement in temperature increases the degree of the dissociation process of ion pairs and affirms the enhancement of free charge carrier concentration at the interface. High temperature may interrupt the ion concentration and ion clusters in the polymer matrix host; thus, the equivalent capacitance increases by forming a space charge region that is exhibiting a high dielectric constant [31, 45].

Figure 13 shows the cyclic voltammogram for the NCPE OCC, (70PEO: 30 [50NaI + 50Na<sub>3</sub>PO<sub>4</sub>]) + 4 ZnO electrolytes. The operating voltage range (i.e., electrochemical potential window) is in the range of  $-3$  to  $3$  V at various scan rates which appear to be rather high for device application, particularly as an electrolyte in sodium rechargeable battery systems [66]. All of the CV curves exhibit more symmetrical peaks, indicating that the produced NCPE OCC film has good electrochemical behavior. The pseudocapacitance behavior of the membranes with the interaction between electrodes and electrolytes is reflected by the existence of peaks in the closed loop [48, 67].

## Conclusion

In the present study, SPEs and NCPEs have been prepared by a novel hot-press method, which is fully flexible and mechanically strong. However, due to the complexation of the binary sodium system and the uniform dispersion of the ZnO nanofiller, XRD investigations show that the amorphous phase of the SPE host and NCPE OCC films have been enhanced in comparison to the host polymer PEO. The smoother surface morphology in NCPE OCC film is confirmed by the SEM

analysis and elemental analysis (EDAX) confirms that all elements are present in the electrolytes. The NCPE OCC film exhibits excellent thermal stability of about 350 °C confirmed by TGA analysis. DSC supports conductivity enhancement of NCPE film which exhibits an improved amorphous nature (about 75.18%) that allows better ion transport; hence the Na<sup>+</sup>-ion conductivity increases. The room temperature conductivity of SPE host, (70PEO: 30 [50NaI + 50Na<sub>3</sub>PO<sub>4</sub>]), is  $\sim 4.89 \times 10^{-6}$  S/cm. However; the most striking finding of this research is that the outstanding effect is the dispersion of the ZnO nano-filler, significantly increasing the ionic conductivity of SPE films  $\sim 1.45 \times 10^{-5}$  S/cm, and surface got uniform and thermal stability also significantly enhanced. Their suitability as an electrolyte/separator for the development of solid-state SIBs is also confirmed by their total ionic transference number  $\sim 0.99$ , which is close to unity. The dielectric constant and dielectric loss are both increasing along with the increasing temperature for NCPE OCC film. The excellent thermal stability of these NCPE films, combined with their high ionic conductivity and electrochemical stability window from  $-3$  to  $+3$  V observed in cyclic voltammetry studies, point to their potential use in the design of all-solid-state Na-ion cells capable of stable operation at temperatures well above room temperature.

**Acknowledgements** All authors acknowledge their sincere thanks to H.O.D., SoS in Physics & Astrophysics, Pt.R.S.U. Raipur and Director, State Forensic Science Laboratory (S.F.S.L.), Raipur (Chhattisgarh) for providing all necessary facilities. One of the authors, Y. K. Mahipal, also acknowledges UGC New Delhi, for UGC-startup grant no. F30-435/2018 (BSR).

**Author contribution** Conceptualization: Niranjana Kumar; methodology: Niranjana Kumar, Y. K. Mahipal; formal analysis and investigation: Niranjana Kumar, Manju Sahu, Dinesh k. Sahu; writing — original draft preparation: Niranjana Kumar] writing — review and editing: Y. K. Mahipal; funding acquisition: nil; resources: Manju Sahu, Dinesh k. Sahu; supervision: Y. K. Mahipal.

**Data availability** The raw/processed data required to reproduce these findings cannot be shared at this time due to technical or time limitations.

## Declarations

**Ethics approval** The submitted manuscript is original work done by the authors and performed in our laboratory. We declare that the manuscript is not considered for publication anywhere.

**Competing interests** The authors declare no competing interests.

## References

- Yang Z, Zhang J, Kintner-Meyer MCW et al (2011) Electrochemical energy storage for green grid. *Chem Rev* 111:3577–3613. <https://doi.org/10.1021/cr100290v>
- Wang Y, Song S, Xu C et al (2021) Development of solid-state electrolytes for sodium-ion battery—a short review. *Elements* 1:91–100. <https://doi.org/10.1016/j.nanoms.2019.02.007>
- Cho J, Jeong S, Kim Y (2015) Commercial and research battery technologies for electrical energy storage applications. *Prog Energy Combust Sci* 48:84–101. <https://doi.org/10.1016/j.pecs.2015.01.002>
- Dunn B, Kamath H, Tarascon JM (2011) Electrical energy storage for the grid: a battery of choices. *Science* 334:928–935. <https://doi.org/10.1126/science.1212741>
- Hasa I, Hassoun J, Passerini S (2017) Nanostructured Na-ion and Li-ion anodes for battery application: a comparative overview. *Nano Res* 10:3942–3969. <https://doi.org/10.1007/s12274-017-1513-7>
- Goodenough JB, Park KS (2013) The Li-ion rechargeable battery: a perspective. *J Am Chem Soc* 135:1167–1176. <https://doi.org/10.1021/ja3091438>
- Yang Q, Zhang Z, Sun XG et al (2018) Ionic liquids and derived materials for lithium and sodium batteries. *Chem Soc Rev* 47:2020–2064. <https://doi.org/10.1039/c7cs00464h>
- Whittingham MS (2004) Lithium batteries and cathode materials. *Chem Rev* 104:4271–4301. <https://doi.org/10.1021/cr020731c>
- Goodenough JB, Kim Y (2010) Challenges for rechargeable Li batteries. *Chem Mater* 22:587–603. <https://doi.org/10.1021/cm901452z>
- Dinachandra Singh M, Dalvi A, Phase DM (2020) Novel Na<sub>3</sub>Zr<sub>2</sub>Si<sub>2</sub>PO<sub>12</sub>-polymer hybrid composites with high ionic conductivity for solid-state ionic devices. *Mater Lett* 262:127022. <https://doi.org/10.1016/j.matlet.2019.127022>
- Komaba S, Murata W, Ishikawa T et al (2011) Electrochemical Na insertion and solid electrolyte interphase for hard-carbon electrodes and application to Na-ion batteries. *Adv Funct Mater* 21:3859–3867. <https://doi.org/10.1002/adfm.201100854>
- Wen X, He C, Wu B et al (2019) Molten salt synthesis, growth mechanism, and photoluminescence of rod chlorapatite microcrystallites. *CrystEngComm* 21:1809–1817. <https://doi.org/10.1039/C8CE02040J>
- Zhao C, Liu L, Qi X et al (2018) Solid-state sodium batteries. *Adv Energy Mater* 8:14–16. <https://doi.org/10.1002/aenm.201703012>
- Kim SW, Seo DH, Ma X et al (2012) Electrode materials for rechargeable sodium-ion batteries: potential alternatives to current lithium-ion batteries. *Adv Energy Mater* 2:710–721. <https://doi.org/10.1002/aenm.201200026>
- Pan H, Hu YS, Chen L (2013) Room-temperature stationary sodium-ion batteries for large-scale electric energy storage. *Energy Environ Sci* 6:2338–2360. <https://doi.org/10.1039/c3ee40847g>
- Hirsh HS, Li Y, Tan DHS et al (2020) Sodium-ion batteries paving the way for grid energy storage. *Adv Energy Mater* 10:1–8. <https://doi.org/10.1002/aenm.202001274>
- Hayashi A, Noi K, Sakuda A, Tatsumisago M (2012) Superionic glass-ceramic electrolytes for room-temperature rechargeable sodium batteries. *Nat Commun* 3:855–856. <https://doi.org/10.1038/ncomms1843>
- Kim J-J, Yoon K, Park I, Kang K (2017) Progress in the development of sodium-ion solid electrolytes. *Small Methods* 1:1700219. <https://doi.org/10.1002/smt.201700219>
- Yang J, Wan HL, Zhang ZH et al (2018) NASICON-structured Na<sub>3.1</sub>Zr<sub>1.95</sub>Mg<sub>0.05</sub>Si<sub>2</sub>PO<sub>12</sub> solid electrolyte for solid-state sodium batteries. *Rare Met* 37:480–487. <https://doi.org/10.1007/s12598-018-1020-3>
- Jinisha B, Anilkumar KM, Manoj M et al (2018) Poly (ethylene oxide) (PEO)-based, sodium ion-conducting, solid polymer electrolyte films, dispersed with Al<sub>2</sub>O<sub>3</sub> filler, for applications in sodium ion cells. *Ionics (Kiel)* 24:1675–1683. <https://doi.org/10.1007/s11581-017-2332-2>



21. Karan S, Sahu M, Sahu TB et al (2017) Investigations on materials and ion transport properties of Zn<sup>2+</sup> conducting nano-composite polymer electrolytes (NCPes): [(90 PEO: 10 Zn(CF<sub>3</sub>SO<sub>3</sub>)<sub>2</sub>)+ x ZnO]. *Mater Today Commun* 13:269–274. <https://doi.org/10.1016/j.mtcomm.2017.10.009>
22. Hashmi SA, Yadav N, Singh MK (2019) Polymer electrolytes for supercapacitor and challenges. *Polym Electrolytes Charact Tech Energy Appl*. <https://doi.org/10.1002/9783527805457.ch9>
23. Qiao L, Judez X, Rojo T et al (2020) Review—polymer electrolytes for sodium batteries. *J Electrochem Soc* 167:070534. <https://doi.org/10.1149/1945-7111/ab7aa0>
24. Dimri MC, Kumar D, Aziz SB, Mishra K (2021) ZnFe<sub>2</sub>O<sub>4</sub> nanoparticles assisted ion transport behavior in a sodium ion conducting polymer electrolyte. *Ionics* 27:1143–1157
25. Sahu TB, Sahu M, Karan S et al (2018) Study of electrical and electrochemical behavior on copper ion conducting nano-composite polymer electrolyte. *Ionics (Kiel)* 24:2885–2892. <https://doi.org/10.1007/s11581-017-2384-3>
26. Cheng S, Smith DM, Li CY (2014) How does nanoscale crystalline structure affect ion transport in solid polymer electrolytes? *Macromolecules* 47:3978–3986. <https://doi.org/10.1021/ma500734q>
27. Glasse MD, Idris R, Latham RJ et al (2002) Polymer electrolytes based on modified natural rubber. *Solid State Ionics* 147:289–294. [https://doi.org/10.1016/S0167-2738\(02\)00024-3](https://doi.org/10.1016/S0167-2738(02)00024-3)
28. Idris R, Glasse MD, Latham RJ et al (2001) Polymer electrolytes based on modified natural rubber for use in rechargeable lithium batteries. *J Power Sources* 94:206–211. [https://doi.org/10.1016/S0378-7753\(00\)00588-7](https://doi.org/10.1016/S0378-7753(00)00588-7)
29. Benedict TJ, Banumathi S, Veluchamy A et al (1998) Characterization of plasticized solid polymer electrolyte by XRD and AC impedance methods. *J Power Sources* 75:171–174. [https://doi.org/10.1016/S0378-7753\(98\)00063-9](https://doi.org/10.1016/S0378-7753(98)00063-9)
30. Noor SAM, Ahmad A, Talib IA, Rahman MYA (2010) Morphology, chemical interaction, and conductivity of a PEO-ENR50 based on solid polymer electrolyte. *Ionics (Kiel)* 16:161–170. <https://doi.org/10.1007/s11581-009-0385-6>
31. Verma ML, Sahu HD (2017) Study on ionic conductivity and dielectric properties of PEO-based solid nanocomposite polymer electrolytes. *Ionics (Kiel)* 23:2339–2350. <https://doi.org/10.1007/s11581-017-2063-4>
32. Ahmad AH, Hassan N, Abrani MA (2014) Preparation and characterization of sodium binary system (NaI-Na<sub>3</sub>PO<sub>4</sub>) inorganic solid electrolyte. *Ionics (Kiel)* 20:389–397. <https://doi.org/10.1007/s11581-013-0988-9>
33. Kaus NH, Ahmad AH (2009) Conductivity studies and ion transport mechanism in LiI-Li<sub>3</sub>PO<sub>4</sub> solid electrolyte. *Ionics (Kiel)* 15:197–201. <https://doi.org/10.1007/s11581-008-0252-x>
34. Agrawal RC, Sahu DK, Mahipal YK, Ashrafi R (2013) Ion transport property of hot-press cast Mg<sup>2+</sup>-ion conducting nano-composite polymer electrolyte membranes: study of effect of active/passive filler particle dispersal on conductivity. *Indian J Pure Appl Phys* 51:320–323
35. Kesharwani P, Sahu DK, Sahu M et al (2017) Study of ion transport and materials properties of K<sup>+</sup>-ion conducting solid polymer electrolyte (SPE): [(1-x) PEO: xCH<sub>3</sub>COOK]. *Ionics (Kiel)* 23:2823–2827. <https://doi.org/10.1007/s11581-016-1872-1>
36. Klongkan S, Pumchusak J (2015) Effects of nano alumina and plasticizers on morphology, ionic conductivity, thermal and mechanical properties of PEO-LiCF<sub>3</sub>SO<sub>3</sub> Solid Polymer Electrolyte. *Electrochim Acta* 161:171–176. <https://doi.org/10.1016/j.electacta.2015.02.074>
37. Gray FM, MacCallum JR, Vincent CA (1986) Poly(ethylene oxide)-LiCF<sub>3</sub>SO<sub>3</sub>-polystyrene electrolyte systems. *Solid State Ionics* 18–19:282–286. [https://doi.org/10.1016/0167-2738\(86\)90127-X](https://doi.org/10.1016/0167-2738(86)90127-X)
38. Hayashi A, Muramatsu H, Ohtomo T et al (2013) Improvement of chemical stability of Li<sub>3</sub>PS<sub>4</sub> glass electrolytes by adding M<sub>x</sub>O<sub>y</sub> (M = Fe, Zn, and Bi) nanoparticles. *J Mater Chem A* 1:6320–6326. <https://doi.org/10.1039/c3ta10247e>
39. Patil SU, Yawale SS, Yawale SP (2014) Conductivity study of PEO-LiClO<sub>4</sub> polymer electrolyte doped with ZnO nanocomposite ceramic filler. *Bull Mater Sci* 37:1403–1409
40. Shin JH, Henderson WA, Passerini S (2003) Ionic liquids to the rescue? Overcoming the ionic conductivity limitations of polymer electrolytes. *Electrochem Commun* 5:1016–1020. <https://doi.org/10.1016/j.elecom.2003.09.017>
41. Ali AMM, Subban RHY, Bahron H et al (2008) Grafted natural rubber-based polymer electrolytes: ATR-FTIR and conductivity studies. *Ionics (Kiel)* 14:491–500. <https://doi.org/10.1007/s11581-007-0199-3>
42. Jinisha B, Km A, Manoj M et al (2017) Development of a novel type of solid polymer electrolyte for solid state lithium battery applications based on lithium enriched poly (ethylene oxide) (PEO)/poly (vinyl pyrrolidone) (PVP) blend polymer. *Electrochim Acta*. <https://doi.org/10.1016/j.electacta.2017.03.118>
43. Wan Z, Lei D, Yang W et al (2019) Low resistance-integrated all-solid-state battery achieved by Li<sub>7</sub>La<sub>3</sub>Zr<sub>2</sub>O<sub>12</sub> nanowire upgrading polyethylene oxide (PEO) composite electrolyte and PEO cathode binder. *Adv Funct Mater* 29:1–10. <https://doi.org/10.1002/adfm.201805301>
44. Pritam AA, Sharma AL (2020) Selection of best composition of Na<sup>+</sup> ion conducting PEO-PEI blend solid polymer electrolyte based on structural, electrical, and dielectric spectroscopic analysis. *Ionics (Kiel)* 26:745–766. <https://doi.org/10.1007/s11581-019-03245-5>
45. Liew CW, Ramesh S, Durairaj R (2012) Impact of low viscosity ionic liquid on PMMA-PVC-LiTFSI polymer electrolytes based on AC -impedance, dielectric behavior, and HATR-FTIR characteristics. *J Mater Res* 27:2996–3004. <https://doi.org/10.1557/jmr.2012.343>
46. Verma ML, Sahu HD (2015) Ionic conductivity and dielectric behavior of PEO-based silver ion conducting nanocomposite polymer electrolytes. *Ionics (Kiel)* 21:3223–3231. <https://doi.org/10.1007/s11581-015-1517-9>
47. Pritam AA, Sharma AL (2019) Dielectric relaxations and transport properties parameter analysis of novel blended solid polymer electrolyte for sodium-ion rechargeable batteries. *J Mater Sci* 54:7131–7155. <https://doi.org/10.1007/s10853-019-03381-3>
48. Vahini M, Muthuvinayagam M (2019) Synthesis and electrochemical studies on sodium ion conducting PVP based solid polymer electrolytes. *J Mater Sci Mater Electron* 30:5609–5619. <https://doi.org/10.1007/s10854-019-00854-8>
49. Agrawal RC, Pandey GP (2008) Solid polymer electrolytes: materials designing and all-solid-state battery applications: an overview. *J Phys D Appl Phys*. <https://doi.org/10.1088/0022-3727/41/22/223001>
50. Hooper A (1977) A study of the electrical properties of single-crystal and polycrystalline β-alumina using complex plane analysis. *J Phys D Appl Phys* 10:1487–1496. <https://doi.org/10.1088/0022-3727/10/11/013>
51. Bowman W, Darbal A, Crozier PA (2019) Linking macroscopic and nanoscopic ionic conductivity: A semiempirical framework for characterizing grain boundary conductivity in polycrystalline ceramics. *ACS Appl Mater Interfaces*. <https://doi.org/10.1021/acsami.9b15933>
52. Angulakshmi N, Yoo DJ, Nahm KS et al (2014) MgAl<sub>2</sub>SiO<sub>6</sub>-incorporated poly(ethylene oxide)-based electrolytes for all-solid-state lithium batteries. *Ionics (Kiel)* 20:151–156. <https://doi.org/10.1007/s11581-013-0985-z>
53. Xi J, Qiu X, Cui M et al (2006) Enhanced electrochemical properties of PEO-based composite polymer electrolyte with shape-selective molecular sieves. *J Power Sources* 156:581–588. <https://doi.org/10.1016/j.jpowsour.2005.06.007>

54. Sathya S, Pazhaniswamy S, Selvin PC et al (2021) Physical and interfacial studies on  $\text{Li}_{0.5}\text{La}_{0.5}\text{TiO}_3$ -incorporated poly(ethylene oxide)-based electrolytes for all-solid-state lithium batteries. *Energy Fuel*. <https://doi.org/10.1021/acs.energyfuels.1c01151>
55. Ibrahim S, Johan MR (2012) Thermolysis and conductivity studies of poly(ethylene oxide) (PEO) based polymer electrolytes doped with carbon nanotube. *Int J Electrochem Sci* 7:2596–2615
56. Maier J (2004) Ionic transport in nano-sized systems. *Solid State Ionics* 175:7–12. <https://doi.org/10.1016/j.ssi.2004.09.051>
57. Xiong HM, Zhao X, Chen JS (2001) New polymer-inorganic nanocomposites: PEO-ZnO and PEO-ZnO- $\text{LiClO}_4$  films. *J Phys Chem B* 105:10169–10174. <https://doi.org/10.1021/jp0103169>
58. Agrawal RC, Chandra A, Bhatt A, Mahipal YK (2008) Investigations on ion transport properties of and battery discharge characteristic studies on hot-pressed  $\text{Ag}^+$ -ion-conducting nano-composite polymer electrolytes:  $(1-x)$  [90PEO: 10 $\text{AgNO}_3$ ]:  $\text{XSiO}_2$ . *New J Phys*. <https://doi.org/10.1088/1367-2630/10/4/043023>
59. Lakshmi N, Chandra S (2001) Proton conducting composites of heteropolyacid hydrates (phosphomolybdic and phosphotungstic acids) dispersed with insulating  $\text{Al}_2\text{O}_3$ . *Phys Status Solidi Appl Res* 186:383–399. [https://doi.org/10.1002/1521-396X\(200108\)186:3%3c383::AID-PSSA383%3e3.0.CO;2-9](https://doi.org/10.1002/1521-396X(200108)186:3%3c383::AID-PSSA383%3e3.0.CO;2-9)
60. Agrawal RC, Gupta RK (1999) Superionic solids: composite electrolyte phase — an overview. *J Mater Sci* 34:1131–1162. <https://doi.org/10.1023/A:1004598902146>
61. Song S, Yang S, Zheng F et al (2016) Communication — poly(ethylene oxide)-immobilized ionogel with high ionic liquid loading and superior ionic conductivity. *J Electrochem Soc* 163:2887–2889. <https://doi.org/10.1149/2.0311614jes>
62. Aziz SB, Woo TJ, Kadir MFZ, Ahmed HM (2018) A conceptual review on polymer electrolytes and ion transport models. *J Sci Adv Mater Devices* 3:1–17. <https://doi.org/10.1016/j.jsamd.2018.01.002>
63. Aziz SB (2013)  $\text{Li}^+$  ion conduction mechanism in poly( $\epsilon$ -caprolactone)-based polymer electrolyte. *Iran Polym J* 22:877–883. <https://doi.org/10.1007/s13726-013-0186-7>
64. Ramya CS, Selvasekarapandian S, Hirankumar G et al (2008) Investigation on dielectric relaxations of PVP- $\text{NH}_4\text{SCN}$  polymer electrolyte. *J Non Cryst Solids* 354:1494–1502. <https://doi.org/10.1016/j.jnoncrysol.2007.08.038>
65. Vinoth Rathan S, Govindaraj G (2010) Thermal and electrical relaxation studies in  $\text{Li}(4+x)\text{Ti}_x\text{Nb}_{1-x}\text{P}_3\text{O}_{12}$  ( $0.0 \leq x \leq 1.0$ ) phosphate glasses. *Solid State Sci* 12:730–735. <https://doi.org/10.1016/j.solidstatesciences.2010.02.030>
66. Kumar D, Hashmi SA (2010) Ionic liquid based sodium ion conducting gel polymer electrolytes. *Solid State Ionics* 181:416–423. <https://doi.org/10.1016/j.ssi.2010.01.025>
67. Muchakayala R, Song S, Gao S et al (2017) Structure and ion transport in an ethylene carbonate-modified biodegradable gel polymer electrolyte. *Polym Test* 58:116–125. <https://doi.org/10.1016/j.polymertesting.2016.12.014>
68. Kamboj V, Arya A, Tanwar S et al (2021) Nanofiller-assisted  $\text{Na}^+$ -conducting polymer nanocomposite for ultracapacitor: structural, dielectric and electrochemical properties. *J Mater Sci* 56:6167–6187. <https://doi.org/10.1007/s10853-020-05667-3>
69. Ji K, Moon H, Kim J, Park J (2003) Role of functional nano-sized inorganic fillers in poly(ethylene) oxide-based polymer electrolytes. *J Power Sources* 117:124–130. [https://doi.org/10.1016/S0378-7753\(03\)00159-9](https://doi.org/10.1016/S0378-7753(03)00159-9)

**Publisher's Note** Springer Nature remains neutral with regard to jurisdictional claims in published maps and institutional affiliations.